Paleoseismic study on active normal faults in the southeastern Weihe Graben, central China

AUTHOR(S):

Rao, Gang; Lin, Aiming; Yan, Bing

(Red color indicating the main revisions)

Paleoseismic study on active normal faults in the southeastern Weihe Graben, central China

Gang Rao[1, 2], Aiming Lin[1,*], Bing Yan[1, 3]

[1]Department of Geophysics, Graduate School of Science, Kyoto University, Kyoto 606-8502, Japan

[2]Department of Earth Sciences, Zhejiang University, Hangzhou 310027, China

[3]School of Earth Sciences and Engineering, Nanjing University, Nanjing 210093, China

****

***Corresponding author:**

Department of Geophysics

Graduate School of Science, Kyoto University

Kyoto 606-8502, Japan

Tel.: 81-75-753-3941

E-mail: slin@kugi.kyoto-u.ac.jp (A. Lin)

Abstract

Field investigations and trench excavations can provide direct and indirect geological evidence for the occurrence of paleo-earthquakes. In this study, we present geological and topographical evidence for the occurrence of great paleo-earthquakes produced by active normal faults in the southeastern Weihe Graben, central China. Field and trench observations, in combination with radiocarbon ages, reveal that: i) four surface-faulting events occurred in the past 4000 years with an average recurrence interval of ~1000 years, which is in contrast with the previously estimated interval of ~2000–2900 years; ii) the most recent fault event is correlated to the 1556 M~8.5 Huaxian earthquake; iii) an alluvial terrace riser that formed at ~5300 yr B.P. has been vertically offset by 9–11 m, indicating an average vertical slip rate of 1.7–2.1 mm/yr in the late Holocene. Our results confirm that normal faults in the southeastern Weihe Graben have been active in the late Holocene as source seismogenic faults, and that these faults have the potential to trigger large earthquakes of M>7 in the future. Therefore, it is important to urgently reevaluate the seismic potential and seismic hazard in the densely populated Weihe Graben region.

Keywords: normal fault, great paleo-earthquake, 1556 M~8.5 Huaxian earthquake, recurrence interval, Weihe Graben, Ordos Block

1. Introduction

Investigations on the seismogenic behavior of active faults, especially during the

Holocene, are important for assessing the seismic hazard in regions with high historical seismicity (e.g., Yeats et al., 1997; Meghraoui et al., 2001; Lin and Guo, 2008; De Pascale and Langridge, 2012). However, geological evidence of paleoseismicity and precise age constraints for past earthquakes are generally lacking, except for limited recordings of human casualties and damage to infrastructure in areas with ancient historical documents, such as China (e.g., CENC, 2007; Lin et al., 2013a). In central China, near the city of Xi'an (an ancient capital on the loess plateau), an earthquake with a large magnitude of ~8.5 (the Huaxian great earthquake) occurred on January 23, 1556 and caused more than 830,000 deaths, making this earthquake the most deadly in history (Kuo, 1957; SSB, 1988; Xie, 1992; CENC, 2007). In the epicentral area between Weinan and Huayin (Fig. 1c), local residents have for thousands of years lived in loess cave dwellings that are susceptible to collapse during earthquakes, and this might explain the great number of deaths.

Although the tectonic activity and structural features of active faults in the epicentral area of the Huaxian great earthquake have been reported previously (e.g., Li and Ran, 1983; SSB, 1988; Zhang et al., 1995; Hou et al., 1998; Yuan and Feng, 2010; Rao et al., 2014), the seismogenic behavior of associated faults remains unclear. Based on field observations of fault scarps and outcrops, previous studies have inferred that the Huashan Piedmont Fault (HPF in Fig. 1c) was the seismogenic fault of the 1556 event (e.g., SSB, 1988; Zhang et al., 1995). However, the paleoseismology of the Northern Margin Fault of the Weinan Loess Tableland (NMF-WLT in Fig. 1c), another important active normal fault located between

Weinan and Huaxian in the southeastern Weihe Graben, remains unknown even though it has been active during the late Pleistocene–Holocene (e.g., Yuan and Feng, 2010; Rao et al., 2014).

In this study, we present a paleo-seismological study on the NMF-WLT and calculate the slip-rate, recurrence interval, and timing of recent faulting events. Then, we discuss the implications of our findings for seismic hazard assessment in the densely populated Weihe Graben region.

2. Geological setting

The Cenozoic intracontinental Weihe Graben is located along the southern margin of the Ordos Block, which is composed mainly of pre-Mesozoic crystalline basement (Ma and Wu, 1987; SSB, 1988). To the south, the graben is bounded by the Qinling Mountains, which were formed in response to the collision between the North China Block (NCB) and South China Block (SCB) in the Triassic (Fig. 1a; Meng and Zhang, 2000; Rastchbacher et al., 2003). Long-term extension since the Eocene (~50 Ma) has caused subsidence, resulting in thick (>7 km) graben sedimentary fill, and the uplift of blocks including the Huashan Mountains and Weinan Loess Tableland (SSB, 1988, Zhang et al., 1998). The Huashan Mountains are composed primarily of pre-Mesozoic metamorphic basement, in contrast to the late Quaternary loess and alluvial sediments of the Weinan Loess Tableland (Fig. 1c). Fission-track dates reveal that uplift of the Huashan Mountains started at ~68.2 Ma and accelerated with an average uplift rate of ~0.19 mm/yr since ~17.8 Ma (Yin et al., 2001). In contrast, major uplift of the Weinan

Loess Tableland occurred after 1.2 Ma (Feng and Dai, 2004). Previous studies have demonstrated that active faults along the northern margins of these uplifted belts are characterized by stepped scarps and dominated by normal slip; the average vertical slip rate on the faults is ~2–3 mm/yr for the late Pleistocene to Holocene (e.g., Li and Ran, 1983; SSB, 1988; Deng et al., 2003; Rao et al., 2014). The development of active normal faults in the Weihe Graben is considered to be related to the pre-existing spreading and rifting of the continental crust due to the variations in lithospheric structures relative to the neighboring Ordos Block and Qinling Mountains (SSB, 1988; Bao et al., 2011; Rao et al., 2014; Lin et al., 2015).

The study area, the southeastern Weihe Graben, has a long historical record of earthquakes dating back more than 2000 years to 780 BC (SEIN, 2011). At least seven M>6 earthquakes have been recorded (Table 1). In the case of the 1556 M~8.5 Huaxian great earthquake, it has been suggested that an active fault zone ruptured along a distance of up to 70 km in the southeastern marginal zone of the Weihe Graben (e.g., Wang, 1980; Xie, 1992; CENC, 2007). Historical documents and previous investigations reveal the epicenter was located between the modern cities of Weinan and Huayin; its intensity was XII, the maximum magnitude measured on the China Seismic Intensity Scale (Fig. 1c; Kuo, 1957; Xie, 1992; CENC, 2007; Deng, 2007; Yuan and Feng, 2010).

3. Study methods

We integrated high-resolution, remote sensing imagery with field work to

investigate the tectonic landforms and structural features related to paleoseismicity along the NMF-WLT (Locs. 1–4; Fig. 1c). We also excavated two trenches on distinct fault scarps along the northern margin of the Weinan Loess Tableland (Locs. 5 and 6 in Fig. 1c). Fault-related structures exposed on trench walls were used to identify fault events. To precisely bracket the timing of fault events, radiocarbon dating of organic-rich trench samples was performed by accelerator mass spectrometry (AMS) at the Institute of Accelerator Analysis Ltd., Japan and at BETA Analysis Inc., USA (Table 2).

4. Outcrop observations

Fault outcrops at Locations 1 and 2 occur on both banks of the Chishuihe River, along an active fault trace at the northern margin of the Weinan Loess Tableland (Fig. 2b). The fault is characterized by fault scarps developed on terrace and loess plateau surfaces (Fig. 2a and b). The T1 terrace is vertically offset by ~10 m across the fault (Fig. 2c). Alluvial deposits of the T1 terrace containing organic soil yield a radiocarbon age of ~5,300 yr B.P. (see Fig. 2b for the sample site). The fault plane at Locations 1 and 2 strikes N40°W and dips 55° to the northeast (Fig. 3a–c). Striations on the fault plane indicate normal slip, consistent with the T1 terrace scarp (Fig. 3d and e).

Along the western segment of the NMF-WLT, approximately 5–10 km from Location 2, two fault outcrops occur where the fault branches into two to three sub-faults (Locs. 3 and 4; Fig. 4a). The fault cuts alluvial terraces of the Weihe River

and its tributary alluvial fans with a maximum vertical offset of ~4.6 m (Fig. 4b).

We observed a ~0.5–0.7-m-wide vertical ground fracture in loess deposits along the scarp at Location 3 (Fig. 4c). Striations on the fracture sidewall indicate normal slip (Fig. 4d and e). Radiocarbon dating of an organic soil that fills the fracture yields an age of ~3,920 yr B.P., which is younger than that of the host loess deposit (~22,480 to ~16,270 yr B.P.) (Fig. 4c; Table 2). Therefore, we infer that the ground fracture developed around~3,920 yr B.P.

At Location 4, ~1 km south of the Weihe River, a 10-m-high fault scarp, striking NW and extending for >1 km (Fig. 4a), cuts the river's lowest terrace (Fig. 5a–c). The terrace is composed of yellow–brown sandy loess intercalated with sandy silt, and these beds have been deformed into broad folds (Fig. 5c–e). In the axis of one syncline, sand–silt layers have been liquefied (Fig. 6). The liquefied sand-silt deposits show an irregular zoning structure including silt-sand, sand, and sand-gravel zones (Fig. 6b, c). Grain size analysis places the sands in a range of 0.1-1.0 mm, known to be prone to liquefaction during seismic ground shaking (e.g., Lin, 1997; Obermeier and Dickenson, 2000), Therefore, we suggest that the irregular zoning structure of liquefied deposits may be formed by multiple strong earthquakes because the liquefied sand-silt deposits would be disturbed and mixed by a large earthquake due to strong ground motion.

Organic soil and calcium carbonate shells from the liquefied beds yield ^{14}C ages ranging from ~36,080 to ~6,360 yr B.P. (Fig. 6c; Table 2). Combining with the distribution features of grain size, and zoning structures of liquefied silt-sand deposits,

the broad ^{14}C ages probably indicate multiple strong earthquakes associated with liquefaction that occurred at this site. Therefore, we suggest the recent seismic faulting event that caused liquefaction occurred after ~6,360 yr B.P. (Fig. 6c; Table 2).

5. Trench investigations

5.1 Trench A

Trench A (Loc. 5; Fig. 4a) was excavated across a fault scarp that cuts several small alluvial fans (Fig. 7a). Along the scarp, we measured vertical offsets of ~1.6 and 0.5 m on older and younger fans, respectively (Fig. 7a and b). We also observed a ground fracture with a strike of N60°E and normal-slip striations on its sidewall (Fig. 7c and d), indicating its development along the main fault plane.

To verify the nature of faulting, a trench ~8 m long and ~4 m deep was excavated at Location 5 (Figs. 8–10). Stratigraphic units (1–8) exposed on the east wall of the trench are composed of surface soil, loess deposits, and silt–sand beds with complex injection veins, as well as colluvium (Figs. 8 and 10). The F1 fault offsets the strata and is itself cut by an injection vein filled with irregular fragments of loess and soil (Figs. 8 and 10b), an indication that repeated seismic events occurred in this location.

The west wall of the trench contains silt–sand beds and colluvium cut by multi-stage injection veins filled with unconsolidated silt-soil matrix and rounded to angular fragments of loess and soil which range from a few millimeters to 10 cm in diameters, showing different colors with the neighboring sediments (Fig. 9). Locally, the injection veins are branched into many veinlets and complex networks (Figs 9 and

10). Three faults (F1–F3) are identified based on deformed and offset stratigraphic units: the F1 and F2 faults cut Units 6 and 7, and the F3 fault cuts Units 2 and 8–11 (Fig. 9b). The strata contain numerous shells and organic-rich soil yielding radiocarbon ages of >43,500 to ~7,670 yr B.P. (Fig. 9b; Table 2). In contrast, radiocarbon ages of near-surface Units 2 and 3 are older than those of the underlying sediments (samples C02 and C14; Fig. 9b); we suggest this inversion of sedimentary units was caused by the collapse of over-steepened fault scarps.

5.2 Trench B

Trench B was excavated across a 1.6-m-high fault scarp along the north margin of the loess plateau near the Weihe River (Fig. 11; see Fig. 4a for the location). Stratigraphic units exposed in the trench are yellow-gray sandy silt, gray silty soil, yellow sandy loess, and dark gray surface soils containing abundant organic-rich soil suitable for radiocarbon dating (Figs. 11 and 12). On the west wall of the trench, six faults (F1–F6) are identified; faults F4–F6 cut older stratigraphic units (Units 13–19), whereas faults F1–F3 faults cut younger strata (Units 1–11) (Fig. 12). A sand–soil vein is injected along the F5 fault plane (Fig. 12b). In contrast with the flat-lying Units 1–10, Units 11–19 are deformed and steeply tilted. Radiocarbon ages for Units 14 and 16 are 19,358 and 30,807 yr B.P., respectively; Unit 5 (an injection vein) yields a radiocarbon age of 2,921 yr B.P. (Fig. 12b; Table 2). In contrast, surface soil Units 3, 5 and 8 are younger at 676–2,590 yr. B.P. (Fig. 12b; Table 2).

5.3 Identification of seismic faulting events

In Trench A, deformed and/or disturbed beds, offset strata, fissure-filled veins, and scarp-collapse deposits were used to identify paleo-seismic faulting events. On the east wall of the trench, the F1 fault offsets Units 2–7, an indication that the associated earthquake occurred after their deposition. The F1 fault plane was later displaced during the seismically induced injection of colluvium which consist of sand-silt fragments varying in diameters and different colors with the neighboring sediments (Figs. 8 and 10a). Therefore, the east wall contains evidence of at least two paleoearthquakes.

Widely distributed gray injection veins in sedimentary Units 2, 4, 7 and 8 are also indicative of seismic events (Figs. 8 and 10c); similar structures, triggered by paleo-earthquakes on pre-existing active faults, have been reported recently (e.g., Lin et al., 2013b, 2014, 2015).

On the west wall, the F1 fault cuts Units 5 and 6 and is overlain by Unit 4; therefore, a seismic faulting event occurred after the formation of Unit 6, but prior to that of Unit 4, between ~42,130 and ~22,280 yr B.P. (Fig. 9b; Table 2). The F2 and F3 faults and their sub-faults cut Units 7 and 8, indicating a faulting event occurred after the deposition of Unit 8 (7,670–23,170 yr B.P.; Fig. 9b; Table 2).

In Trench B, at least six seismic events can be identified, five of which occurred in the late Holocene. On the west wall, the F5 and F6 faults cut Units 14–18, indicating that at least one seismic faulting event occurred after the formation of Unit 14, between 30,807 and 19,358 yr B.P. (Fig. 12b; Table 2). The presence of a surface

soil vein (Unit 15) injected into Unit 14 indicates that another faulting event (Ea1) occurred after the injection of Unit 15 at 2,921 yr B.P. (Fig. 12b; Table 2).

As shown in Fig. 12, younger sedimentary units (Units 1–10) are sharply fault-bounded with older sedimentary units (11–19). Unit 10 is steeply (64°) bounded by the F2 fault, cut by the F1 fault, and overlain by a brown-gray surface soil (Unit 8). We suggest the following sequence of events following the development of fault F2: i) a fault event (Eb1) occurred along the high-angle scarp, prompting scarp collapse and the deposition of Unit 10; ii) a fault event (Eb2) occurred just prior to the deposition of Unit 8 at 2,590 yr B.P. (Fig. 12b; Table 2); iii) a fault event (Eb3) occurred along fault F2 that bounds Units 6 and 7, after the deposition of Unit 8 and prior to the deposition of Unit 5 (Fig. 12b; Table 2); and iv) a fault event (Eb4) that occurred after the deposition of Unit 2 (676 ± 23 yr B.P.; Fig. 12b; Table 2). Three surface soil layers (Units 3, 5, and 8), which are sedimentary markers of seismic activity, were formed after individual faulting events, yielding an average recurrence interval of ~1000 years.

Previous studies show that there is a general tendency that strong to large earthquakes in extensional regime usually ruptured on one or some of the fault segments of the associated active faults (McCalpin, 2009). It is possible that some events occurred at one site and not at the other due to discontinuous distribution of coseismic displacement and complicated geometry of faults. In this study, we also found that there is no similar seismic event identified from different sites. This discrepancy may also reflect hiatuses in deposition due to small vertical offsets and

ground subsidence during the paleoseismic events. Therefore, to precisely bracket the timing of fault events, multiple trench sites are usually chosen to make the comparison of paleo-earthquakes identified from each sites.

In summary, trench investigations reveal that four surface faulting events occurred in the past ~4000 years, with a recurrence interval of ~1000 years.

6. Discussion and conclusions

6.1 Recurrence interval of normal-slip earthquakes

We calculated the recurrence interval of successive late Holocene earthquakes based on topographic relationships, deformation features, and ^{14}C ages along active normal faults in the study area. Topographic profiles show that the T1 terrace (5,300 yr B.P.) has a vertical offset of ~10 m (Fig. 2b). Previous work has shown that the 1556 M 8.5 Huaxian great earthquake caused an average vertical offset of ~2–3 m (SSB, 1988). If we use 2–3 m as a characteristic offset for individual great earthquakes in this area, then a total offset of 10 m is inferred to be the sum result of three to five large earthquakes over the past ~5,000 years. Liquefaction of alluvial sand and silt at Location 4 also indicates that at least one faulting event occurred in the past ~6,300 years (Fig. 6).

Multiple late Pleistocene (~20,000–45,000 yr B.P.) and one Holocene (<7,670 yr B.P.) faulting events are identified in Trench A (Fig. 9b). However, in Trench B we identify four surface faulting events over the past ~4000 years, with a recurrence

interval of ~1000 years. The Ea1 event occurred at ~2,921 yr B.P. based on the age of a surface soil vein injected into Unit 14 (Fig. 12b). The Eb1 event occurred just prior to the formation of Unit 10. Using an average recurrence interval of ~1000 years over the past 3,000 years, we infer that the Eb1 event occurred at ~4,000 yr B.P. We also infer that the Eb2 event occurred before the formation of Unit 8 (~2,590 yr B.P.) and may correspond to the Ea1 event that occurred at 2,921 yr B.P. (Fig. 12b; Table 2). The Eb3 event occurred between 1,145 and 2,590 yr B.P., which are the ages of Units 8 and 5, respectively. The Eb4 event is inferred to be the most recent event, occurring in the past 676 years (1360–1388 AD).

Historical documents record seven large M≥6 earthquakes in the Weihe Graben over the past ~3,000 years, including the 1556 M~8.5 Huaxian great earthquake and two large earthquakes of M≥7 (1501 AD and 780 BC; Table 1). However, previous work showed that surface rupturing in the graben systems around the Ordos Block is generally related to M>7 earthquakes (SSB, 1988). For example, the 1996 M6.4 Baotou earthquake did not produce a surface rupture in the Hetao Graben (Li, 2005). Based on historical records, the epicenter of the 1501 M~7 Chaoyi earthquake was near Dali city in the eastern Weihe Graben (SEIN, 2011). Recent study shows that the 1501 Chaoyi earthquake probably occurred in the Shanxi Graben, northeast of the Weihe Graben (Lv et al., 2014). Consequently, only two large historical earthquakes (i.e., the M~7 780 BC Qishan and M~8.5 1556 Huaxian great earthquakes) are associated with active faults in the Weihe Graben.

Therefore, we consider the most recent event (Eb4; 1360–1388 AD) to correspond

285 to the M~8.5 1556 Huaxian great earthquake. The Eb3 event occurred between 1,145
286 and 2,590 yr B.P. Considering the range of ^{14}C dating errors, the Eb3 event might be
287 correlated with the 793 AD earthquake of M~6.5. The magnitude of historical
288 earthquake is generally estimated from the seismic intensity that is inferred from the
289 historical record. The magnitude (M~6.5) of the 793 AD earthquake may be
290 underestimated due to the lack of historical documents recorded one thousand years
291 ago. To better understand this event, more work is needed. The Eb2 event occurred
292 between 2,591 and 2,921 yr B.P. and may be related to the M~7 780 BC earthquake.
293 The demonstrated seismic faulting events including the Eb4, Eb3, and Eb2 are mostly
294 in agreement with the historical documents recorded since 780 BC (Table 1). Since
295 the 1556 earthquake, no strong earthquake has occurred in the study area. Many active
296 faults are distributed throughout regions neighboring the study area, with similar
297 potential to trigger large earthquakes and significant ground deformation (Lin et al.,
298 2015, this issue). Therefore, more work is required to better understand the recurrence
299 interval of large earthquakes and their deformation characteristics, and thereby
300 improve ongoing assessments of seismic hazards in the densely populated Weihe
301 Graben region.
302
303 ***6.2 Rate of normal slip***
304 Although previous studies have described fault outcrops along the NMF-WLT
305 (e.g., Yuan and Feng, 2010; Rao et al., 2014), the rate of fault slip remains poorly
306 constrained, making it difficult to assess the potential seismic hazard. Here, we use

307 topographic analysis of displaced terraces and ^{14}C ages to calculate an accumulated
308 vertical offset of ~9–11 m on the T1 terrace since ~5,300 yr B.P. (Fig. 2; Table 2).
309 Striations on the main fault plane indicate nearly pure normal slip (Fig. 3). Therefore,
310 we estimate the average rate of fault slip on the NMF-WLT to be ~1.7–2.1 mm/yr
311 during the Holocene. This result is consistent with a previous estimate for late
312 Pleistocene slip of ~2–3 mm/yr for the epicenter of the 1556 Huaxian great
313 earthquake (e.g., Li and Ran, 1983; Deng et al., 2003; Rao et al., 2014) and also
314 agrees with a slip estimate of ~0.5–1.1 mm/yr for active normal faults in the
315 northwestern Weihe Graben (Lin et al. 2015, this issue). Coupling an average slip rate
316 of ~2 mm/yr with a single-event offset of ~2 m (characteristic of M7–8 earthquakes in
317 the study area), the recurrence interval of M7–8 earthquakes is ~1000 years,
318 consistent with the recurrence interval estimated from trench investigations.
319

320 **Acknowledgements**

321 We thank the Earth Remote Sensing Data Analysis Center (ERSDAC) for making
322 ASTER GDEM data freely available. We are grateful to Profs. D. Jia and J. Hu, and
323 Drs. Z. Ren, X. Wu, J. Fu, J. Du, H. Chen, and W. Gong for discussions and help in
324 the field. Thanks also due to Prof. H. Li and Dr. Z. Wang for their valuable critical
325 reviews that greatly improved the manuscript. This work was supported by the
326 Science Project (23253002) from the Ministry of Education, Culture, Sports, Science
327 and Technology of Japan and partially by the Fundamental Research Funds for the
328 Central Universities (No. 2014QNA3010).

329

References

CENC (China Earthquake Network Center), 2007, The 1556 Huaxian great earthquake, Shaanxi, China: the largest total of fatalities ever claimed (in Chinese). Available online at: http://www.csi.ac.cn/manage/html/4028861611c5c2ba0111c5c558b00001/_history/hxz/qyzhenhai/zh20060609002.htm (Last accessed, 30 August 2014)

Deng, Q., Zhang, P., Ran, Y., Yang, X., Min, W., Chu, Q., 2003. Basic characteristics of active tectonics of China. Sci. China Ser. D 46, 356–372.

Deng, Q., 2007. Active Tectonics Map of China, Seismological Press (in Chinese).

De Pascale, G., Langridge, R., 2012. New on-fault evidence for a great earthquake in A.D. 1717, central Alpine fault, New Zealand. Geology 40, 791–794.

Feng, X., Dai, W., 2004. Lateral migration of fault activity in Weihe basin. Acta Seismologica Sinica 17, 190–199.

Geological Bureau of Shaanxi Province (GBSP), 1999. Regional Geology of Shaanxi Province, China Geological Survey, Beijing.

Hou, J., Han, M., Chai, B., Han, H., 1998. Geomorphological observations of active faults in the epicentral region of the Huaxian large earthquake in 1556 in Shaanxi Province, China. J. Struct. Geol. 20, 549–557.

Kuo, T., 1957. On the Shensi earthquake of January 23, 1556. Acta Geophysica Sinica, 6, 59–68 (in Chinese with English abstract).

Li, J., 2005. Research on the satellite remote sensing images indicative of strong earthquake preparation in the Ordos north marginal fault basin region.

352 Seismology and Geology 3, 374–381 (in Chinese with English abstract).
353 Li, X., Ran, Y., 1983. Active faults along the north margins of Huashan and Weinan
354 Loess Tableland. North China Earthquake Science 1, 10–18 (in Chinese with
355 English abstract).
356 Lin, A., 1997. Instantaneous-shaking liquefaction induced by the M7.2 1995 Southern
357 Hyogo Prefecture earthquake, Japan. Geology 25, 435–438.
358 Lin, A., Guo, J., 2008. Non-uniform slip rate and millennial recurrence interval of
359 large earthquakes along the eastern segment of the Kunlun fault, northern Tibet.
360 Bull. Seismol. Soc. Am. 98, 2866–2878.
361 Lin, A., Rao, G., Hu, J., Gong, W., 2013a. Reevaluation of the offset of the Great Wall
362 caused by the ca. M 8.0 Pingluo earthquake of 1739, Yinchuan graben, China. J.
363 Seismol. 17, 1281–1294.
364 Lin, A., Yamashita, K., Tanaka, M., 2013b. Repeated seismic slips recorded in
365 ultracataclastic veins along active faults of the Arima–Takatsuki Tectonic Line,
366 southwest Japan. J. Struct. Geol. 48, 3–13.
367 Lin, A., Rao, G., Yan, B., 2014. Structural analysis of the right-lateral strike-slip
368 Qingchuan fault, northeastern segment of the Longmen Shan thrust belt, central
369 China. J. Struct. Geol. 68, 227–244.
370 Lin, A., Rao, G., Yan, B., 2015. Flexural fold structures and active faults in the
371 northern-western Weihe Graben, central China. J. Asian. Earth Sci., this issue.
372 Lv, S., Li, Y., Wang, Y., Ci, H., 2014. The Holocene paleoseismicity of the North
373 Zhongtiaoshan Faults in Shanxi Province, China. Tectonophysics 623, 67–82.

374 Ma, X., Wu, D., 1987. Cenozoic extensional tectonics in China. Tectonophysics 133,
375 243-255.
376 McCalpin, J.P., 2009. Paleoseismology, Second edition. International geophysics
377 series, vol. 95. Academic Press (613 pp).
378 Meghraoui, M., Delouis, B., Ferry, M., Giardini, D., Huggenberger, P., Spottke, I.,
379 Granet, M., 2001. Active normal faulting in the Upper Rhine graben and
380 paleoseismic identification of the 1356 Basel earthquake. Science 293,
381 2070–2073.
382 Meng, Q., Zhang, G., 2000. Geologic framework and tectonic evolution of the Qinling
383 orogen, central China. Tectonophysics 323, 183–196.
384 Obermeier, S.F., Dickenson, S.E., 2000. Liquefaction evidence for the strength of
385 ground motions resulting from late Holocene Cascadia subduction earthquakes,
386 with emphasis on the event of 1700 A.D. Bull. Seismol. Soc. Am. 90, 876–896.
387 Rao, G., Lin, A., Yan, B., Ren, Z., Jia, D., Wu, X., 2014. Tectonic activity and
388 structural features of active intracontinental normal faults in the Weihe Graben,
389 central China. Tectonophysics 638, 270–285.
390 Ratschbacher, L., Hacker, B., Calvert, A., Webb, L., Grimmer, J., McWilliams, M.,
391 Ireland, T., Dong, S., Hu, J., 2003. Tectonics of the Qinling (Central China):
392 tectonostratigraphy, geochronology, and deformation history. Tectonophysics 366,
393 1–53.
394 Shaanxi Earthquake Information Network (SEIN), 2011. Historical earthquakes in
395 Shaanxi province (in Chinese). Available online at: http://

http://www.eqsn.gov.cn/manage/html/8abd83af1c88b3f2011c88b74299001f/sxlsdz/index.html (Last accessed, 30 August 2014).

State Seismological Bureau (SSB), 1988. Active fault system around Ordos Massif (in Chinese). Seismological Press, Beijing, (352 pp.).

Stuiver, M., Reimer, P.J., Reimer, R., 2005. CALIB radiocarbon calibration version 7.0.http://radiocarbon.pa.qub.ac.uk/calib/ (Last accessed, 30 August 2014).

Wang, J., 1980. Ground ruptures during the large earthquake of 1556, Huaxian County, Shanxi. Acta Seismologica Sinica 2, 430–437 (in Chinese with English abstract).

Xie, Y., 1992. On magnitude of 1556 Guanzhong great earthquake. Journal of Catastrophology 7, 10–13 (in Chinese with English abstract).

Yeats, R., Seih, K., Allen, C., 1997. The Geology of earthquakes. Oxford University Press, Oxford (568 pp.).

Yin, G., Lu Y., Zhao, H., Li, W., Li, L., Guo, S., 2001. The tectonic uplift of the Hua Shan in the Cenozoic. Chin. Sci. Bull. 46, 1665–1668.

Yuan, T., Feng, X., 2010. The 1556 Huaxian great earthquake (in Chinese), Seismological Press, Beijing (386 pp.).

Zhang, A., Yang, Z., Zhong, J., Mi, F., 1995. Characteristics of late quaternary activity along the Southern Border Fault Zone of Weihe Graben Basin. Quatern. Int. 25, 25–31.

Zhang, Y., Mercier, J.L., Vergély, P., 1998. Extension in the graben systems around the Ordos (China), and its contribution to the extrusion tectonics of south China with respect to Gobi-Mongolia. Tectonophysics 285, 41–75.

418

419 **Figure captions**

420 **Figure 1** (a) Geology of graben systems around the Ordos Block; (b) color-shaded
421 relief map showing topographic features and the distribution of major active
422 faults and historical earthquakes (modified from Deng, 2007); (c) geological map
423 of the study area (modified from GBSP, 1999). The red star is the epicenter of the
424 1556 Huaxian great earthquake (CENC, 2007). ATF: Altyn Tagh Fault; HYF:
425 Haiyuan Fault; KLF: Kunlun Fault; GZ-YSF: Ganzi-Yushu Fault; XSHF:
426 Xianshuihe Fault; LMS: Longmenshan; NCB: North China Block; SCB: South
427 China Block; QLF: Qinling Fault; HPF: Huashan Piedmont Fault; NMF-WLT:
428 Northern Margin Fault of Weinan Loess Tableland; LPF: Lishan Piedmont Fault;
429 KGF: Kouzhen-Guanshan Fault; WF: Weihe Fault.

430 **Figure 2** (a) South-looking oblique 1-m IKONOS image of the Chishuihe region; (b)
431 geological interpretation of the image; (c) topographic profiles across the fault
432 scarp.

433 **Figure 3** (a, b) Active faults displacing river banks (Locs. 1 and 2); (c) fault gouge; (d)
434 striations observed along the main fault plane; (e) orientations of striations on the
435 fault plane (lower hemisphere equal-arc stereographic projection), indicating
436 normal-dominated slip.

437 **Fig. 4** (a) South-looking oblique 1-m IKONOS image of the eastern Weinan area; (b)
438 a 4.6-m-high fault scarp (Loc. 3); (c) ground fractures beneath the scarp; (d, e)
439 striations on the sidewall indicating dip-slip motion.

440 **Figure 5** (a, b) A 10-m-high fault scarp at Loc. 4; (c–e) tilted strata with internal

441 bedding and a fault deformation zone composed of sub-parallel fault planes.

442 **Figure 6** (a) Sketch of the outcrop at Loc. 4; (b, c) sand liquefaction; (d) grain-size
443 distribution of boiled sands.

444 **Figure 7** (a) Trench A, excavated across a 0.5–1.6-m-high fault scarp at Loc. 5; (b)
445 ground fracture beneath the scarp; (c, d) striations on the sidewall indicate
446 dip-slip motion.

447 **Figure 8** (a) Photograph and (b) corresponding sketch of the east wall in Trench A.

448 **Figure 9** (a) Photograph and (b) corresponding sketch of the west wall in Trench A.

449 **Figure 10** Characteristic deformation and sedimentary features observed on the
450 exposed walls in Trench A. (a) Colluvium; (b) fault plane displaced by injected
451 colluvium; (c) injected veins; (d) cross-cutting veins.

452 **Figure 11** (a, b) Trench B, excavated across a 1.6-m-high fault scarp at Loc. 6; (c)
453 overview of trench walls and exposed sedimentary layers.

454 **Figure 12** (a) Photograph and (b) corresponding sketch of the west trench wall
455 exposed in Trench B.

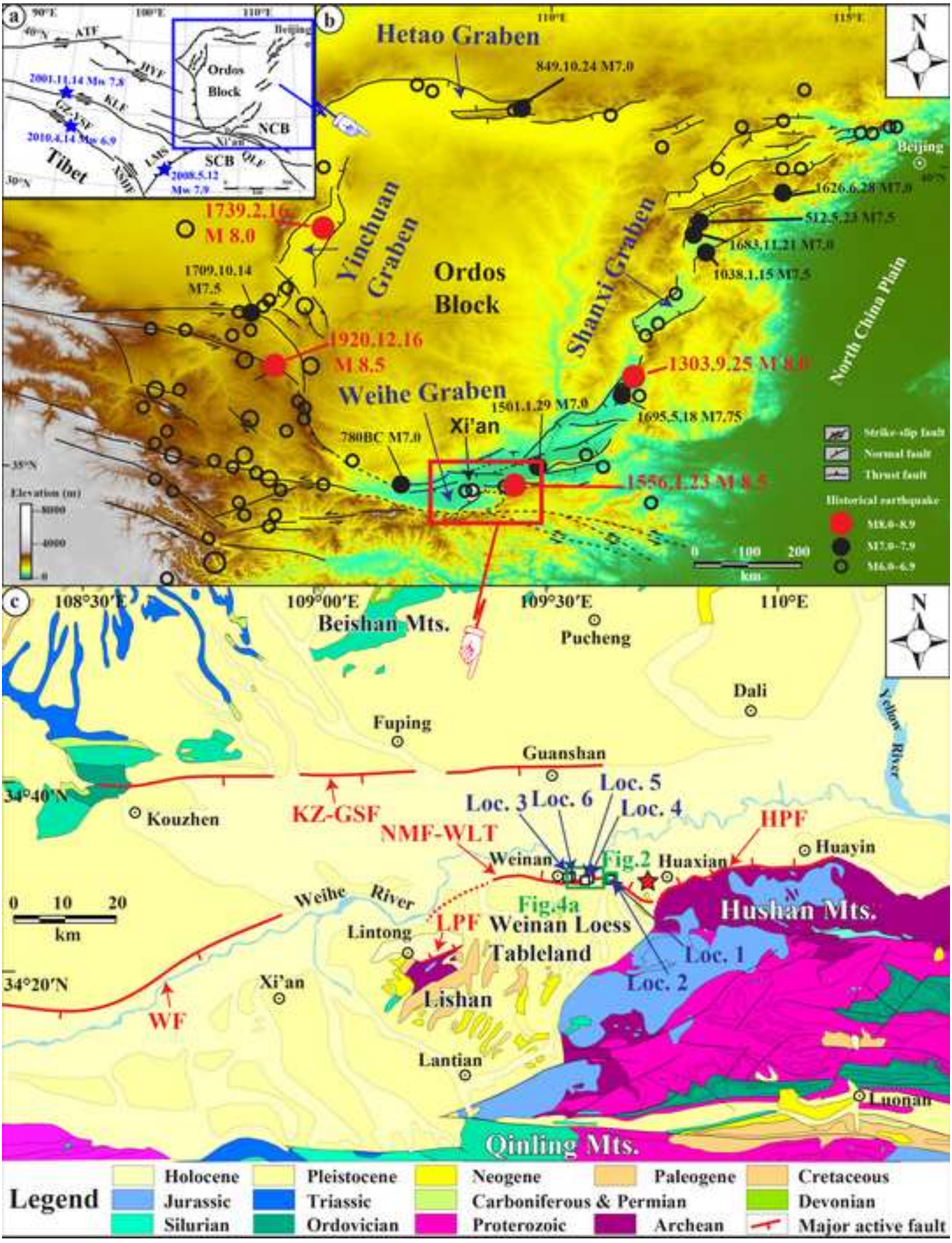

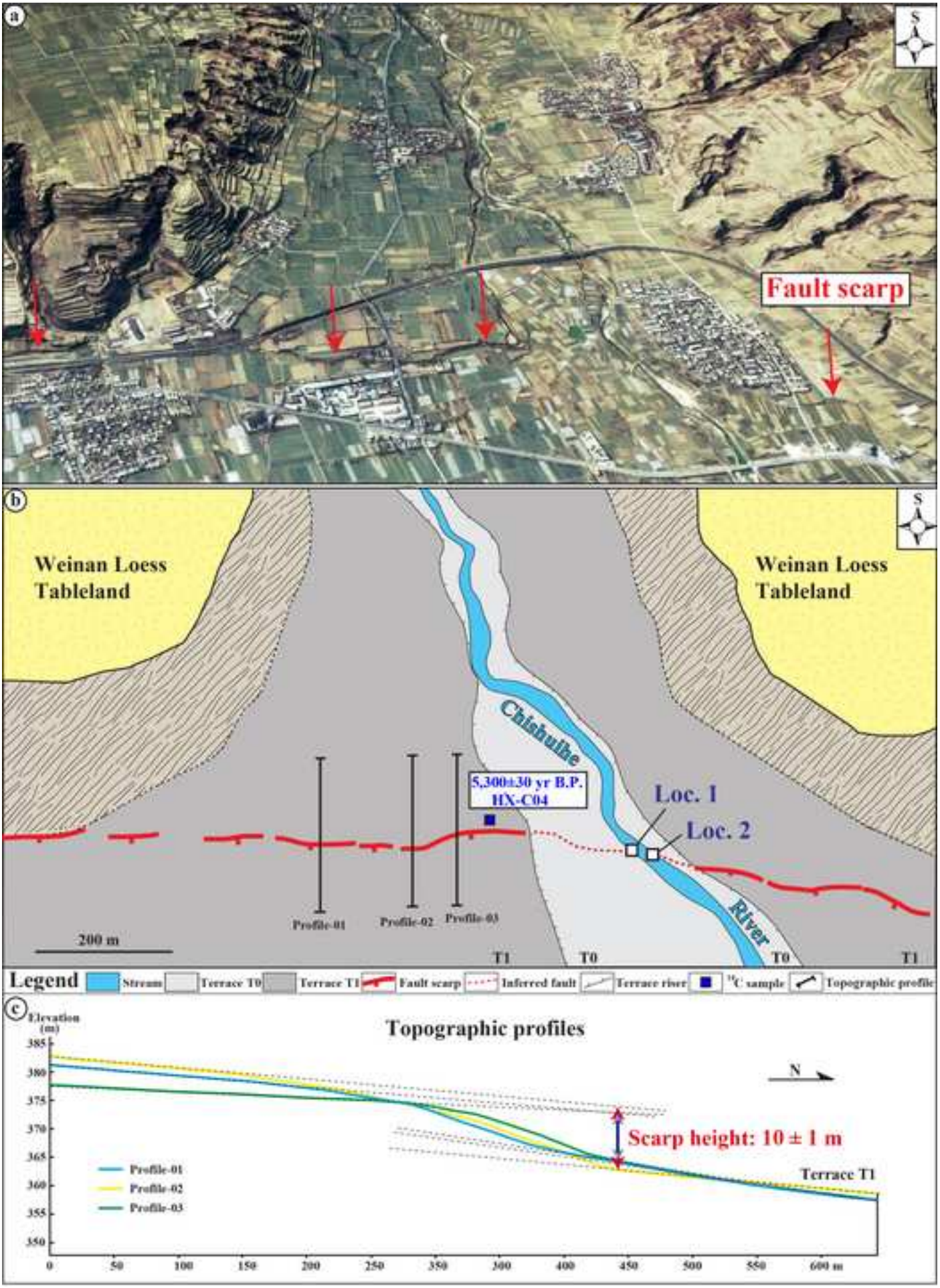

Figure3

Click here to download high resolution image

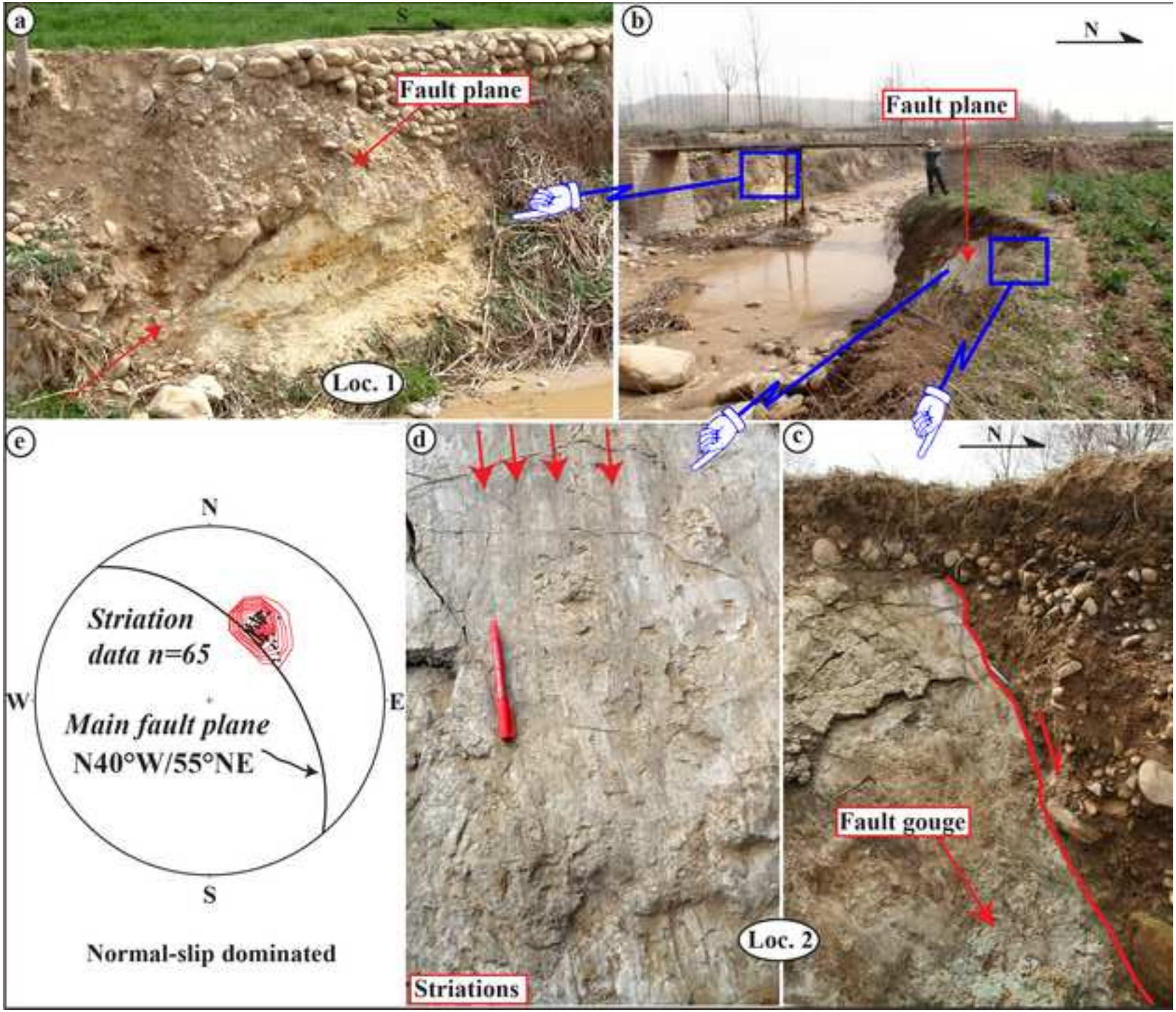

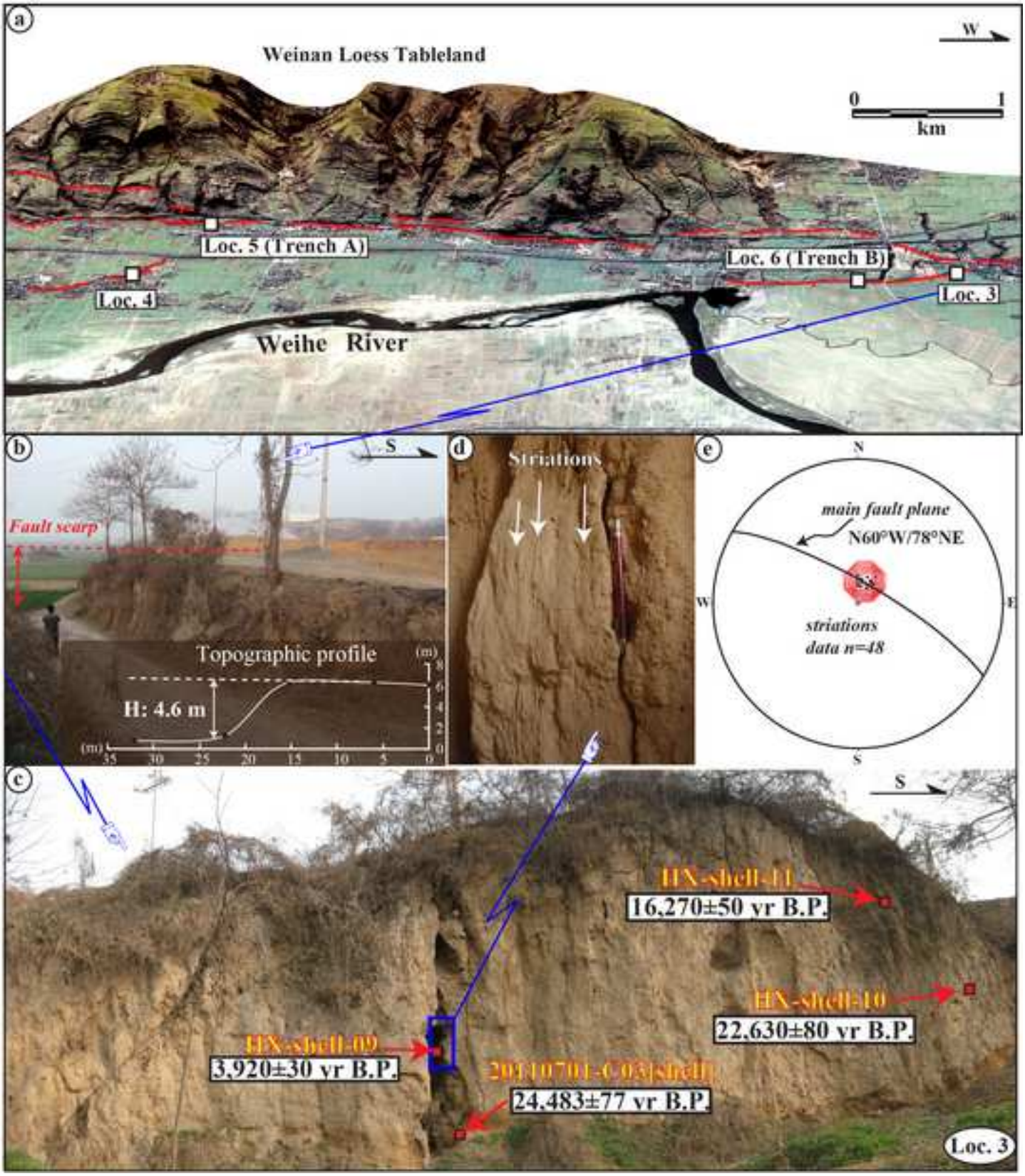

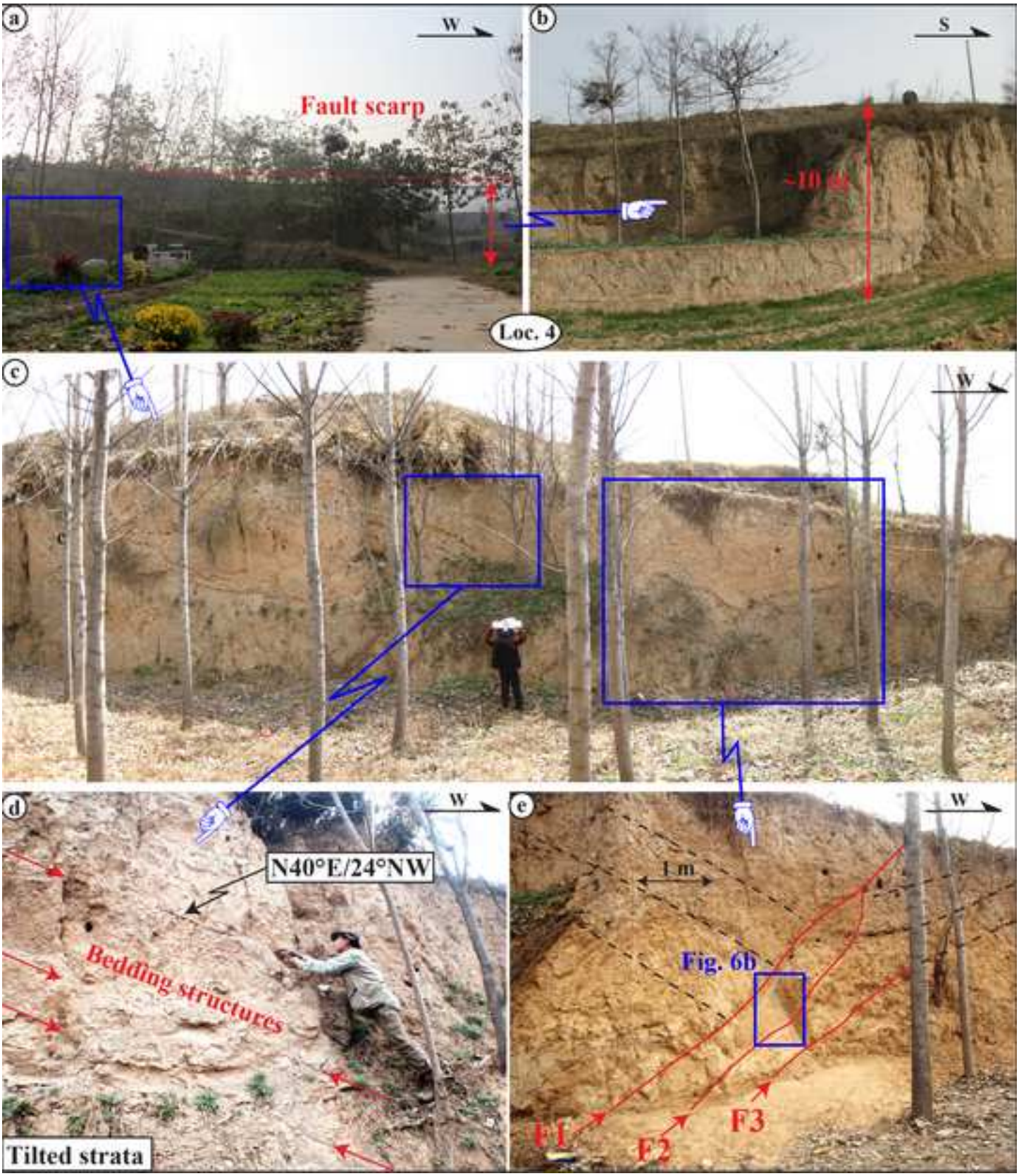

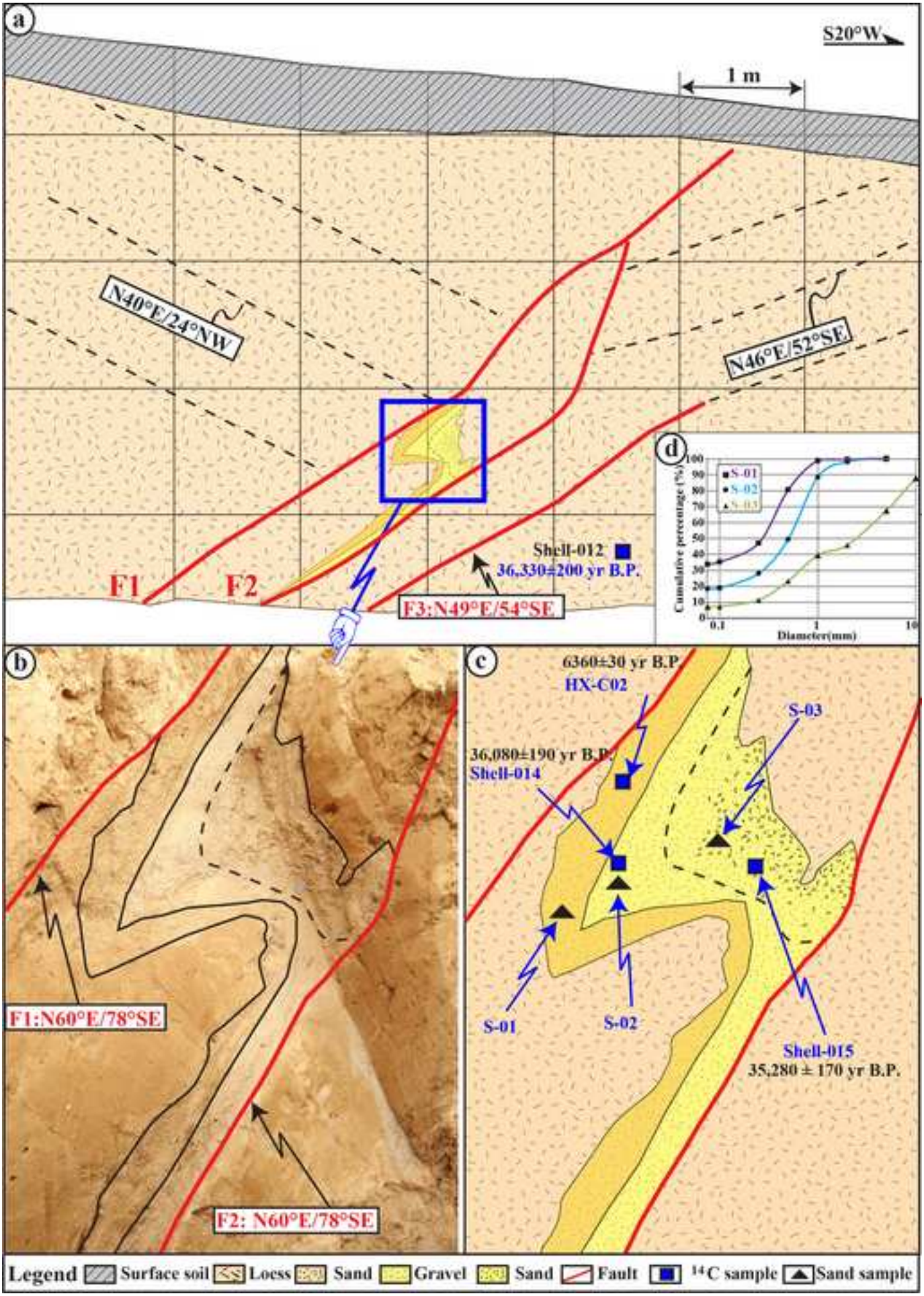

Figure7

Click here to download high resolution image

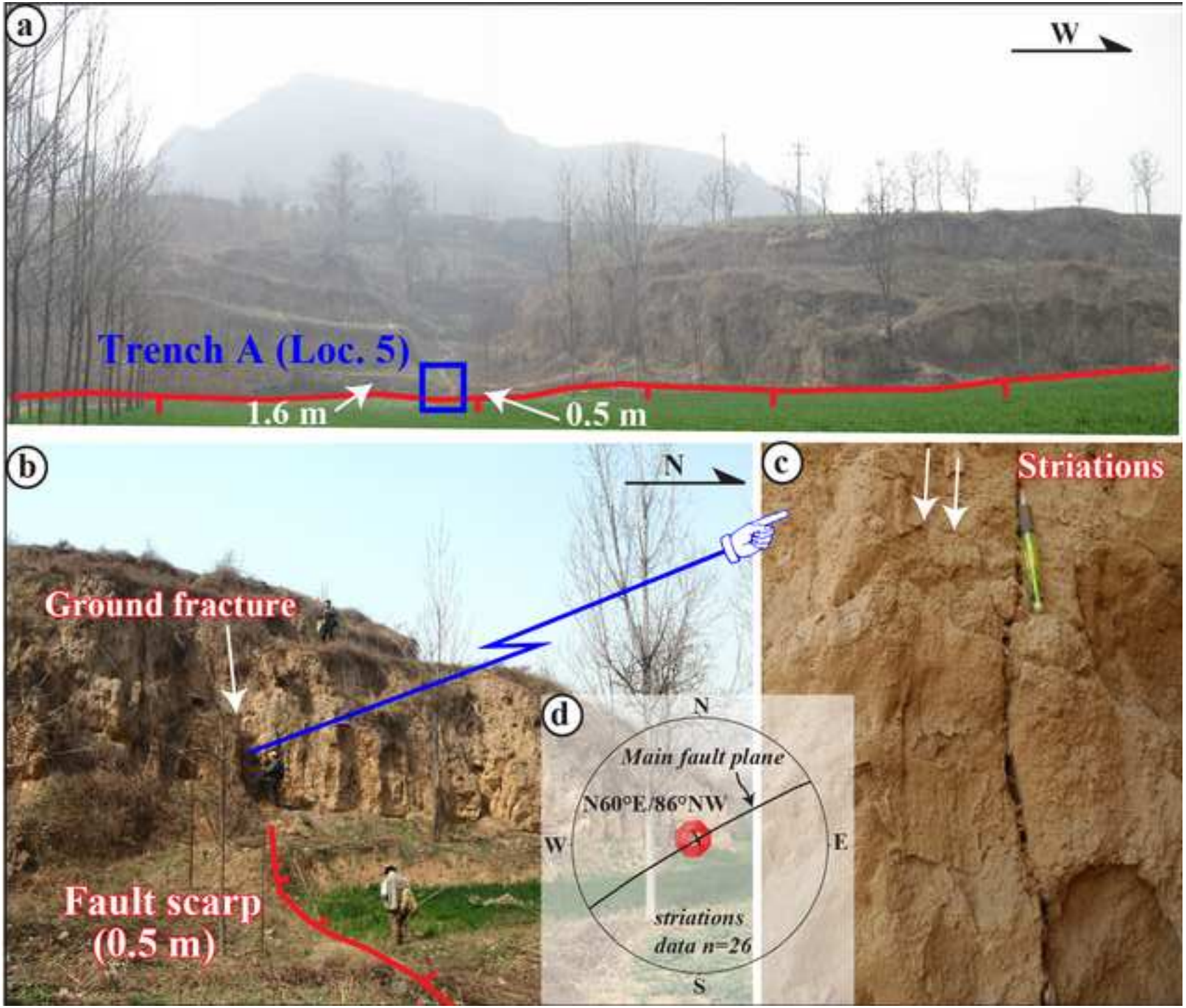

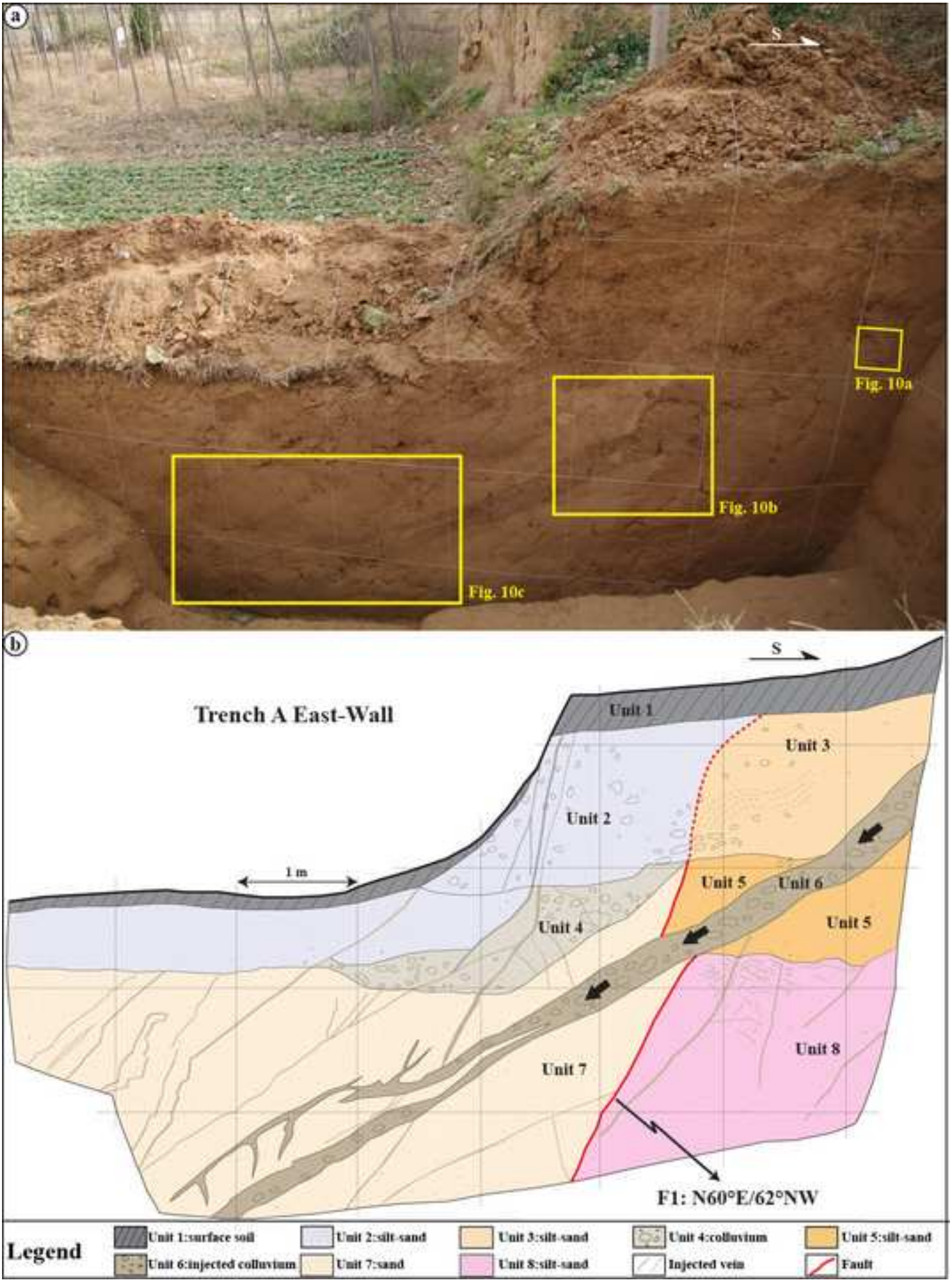

Figure9

Click here to download high resolution image

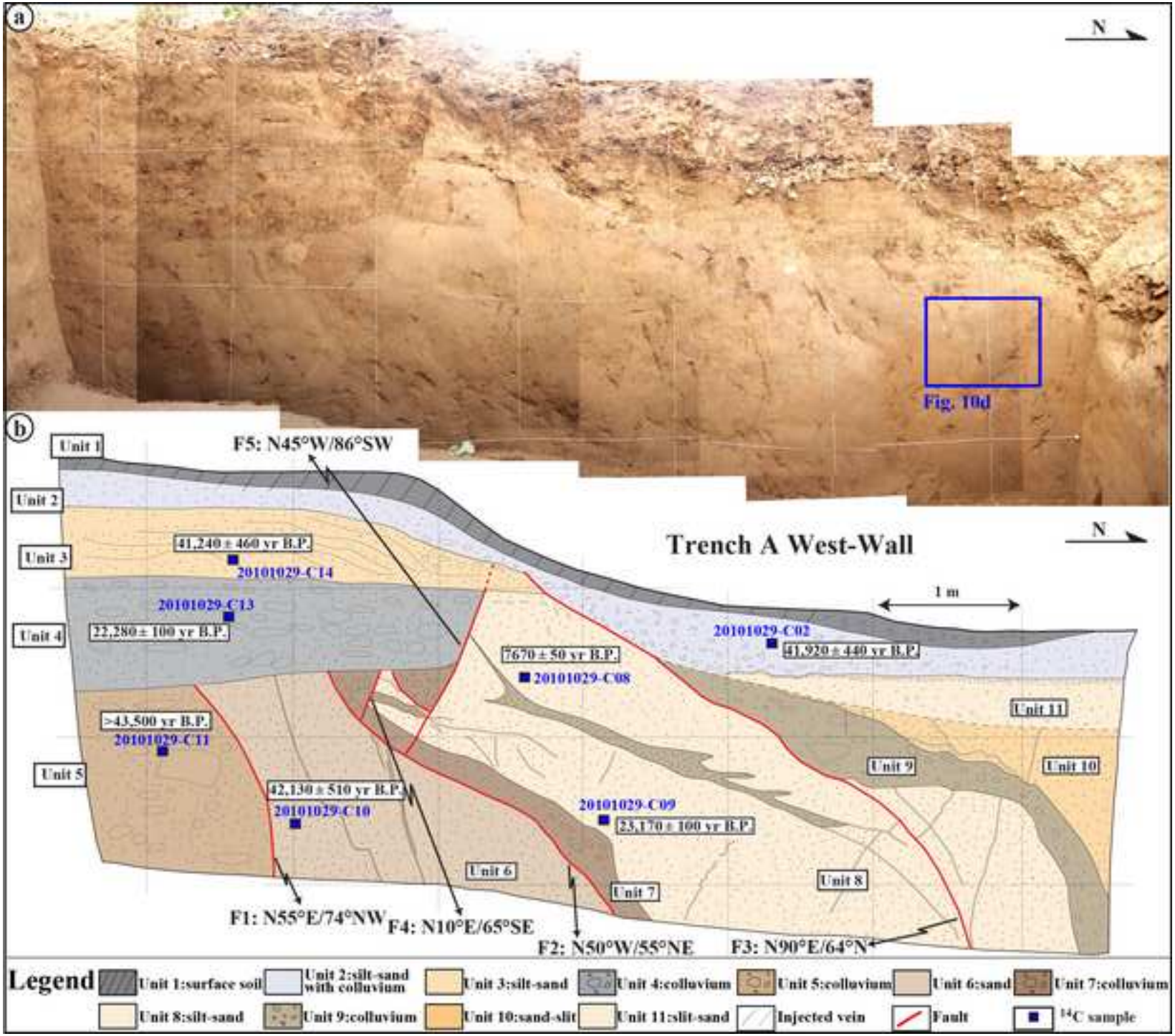

Figure10

Click here to download high resolution image

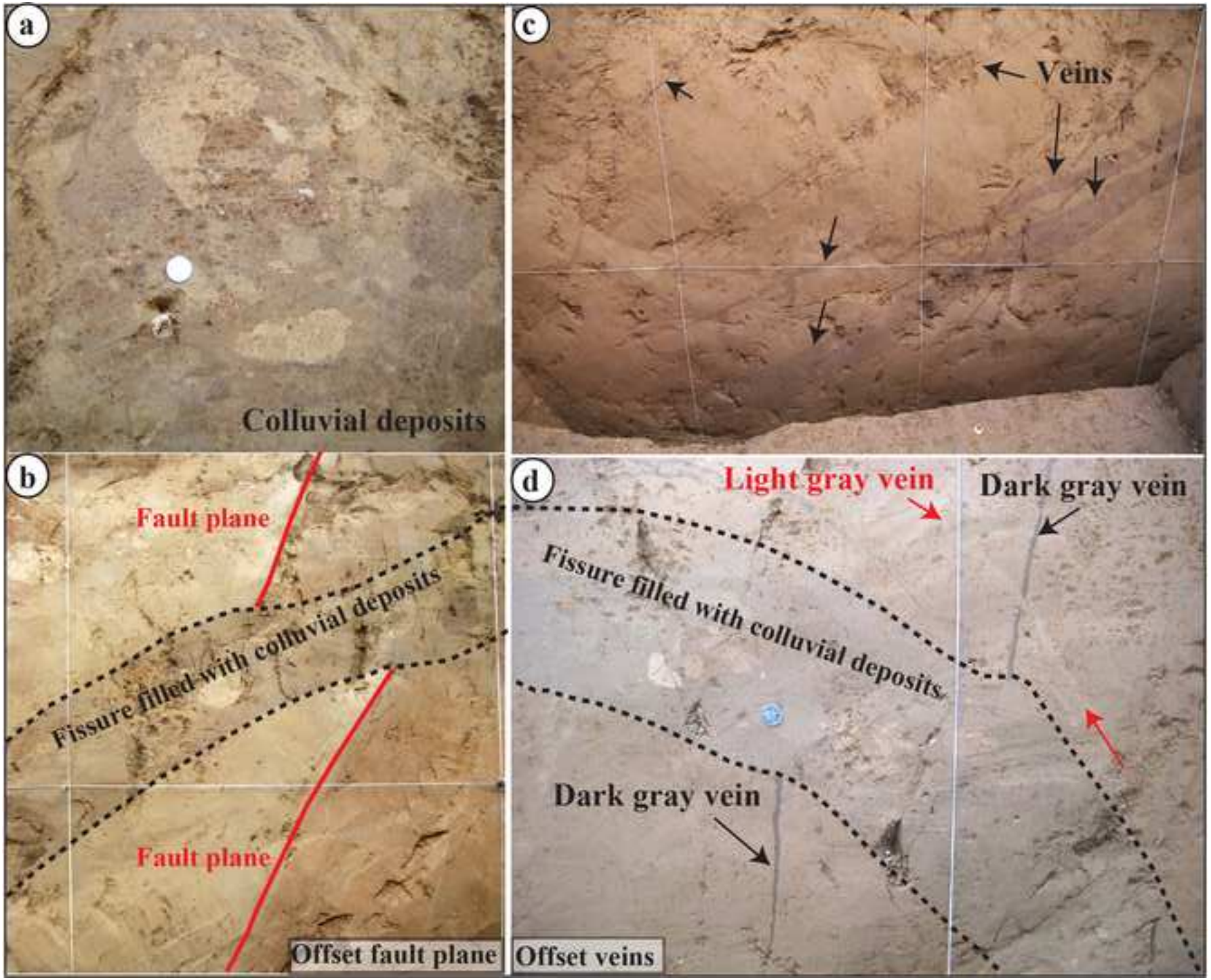

Figure11

Click here to download high resolution image

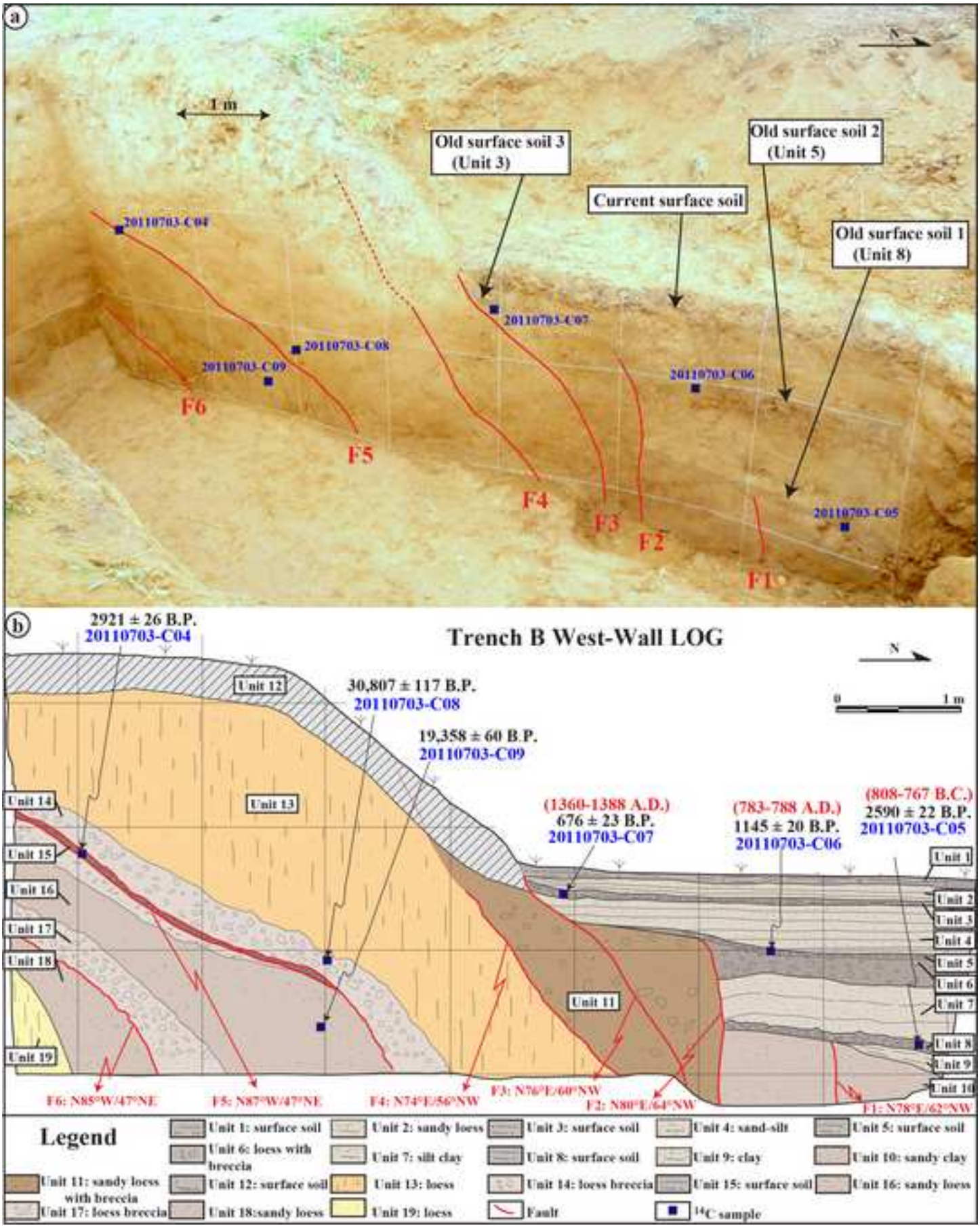

Table 1 Historical earthquakes of M≥6 in Weihe Graben.

Date	***Location***	***Magnitude***	***References***
AD 1568.7.5	Xi'an	~6.75	EBASP, 1989; SEIN, 2011;
AD 1556.1.23	Huaxian	~8.5	e.g. Kuo, 1957; Wang, 1980; SSB, 1988; Xie, 1993; Zhang et al., 1995; Hou et al., 1998; Yuan and Feng, 2010;
AD 1501.1.19	Chaoyi	~7	Wang, 1985; Wang et al., 2004; SEIN, 2011;
AD 1487.8.10	Lintong	~6.25	Wang, 1985, EBASP, 1989;
AD 793.5.27	Weinan	~6.5	Wang, 1985; EBASP, 1989; SEIN, 2011;
BC 7.11.11	Northeast to Xi'an (?)	~6	Wang, 1985; EBASP, 1989;
BC 780	Qishan, Huaxian (?)	~7	Wang, 1985; EBASP, 1989; SEIN, 2011.

Table 2 Radiocarbon age data for samples collected in Weihe Graben.

Sample code	*Laboratory ID*[*]	*Radiocarbon age (yr B.P.)*[†]	Calibrate age (2σ uncertainties)[‡]	*Description*[§]
HX-C02	IAAA-100062*	6,360 ± 30		Shell; Loc. 4; Fig. 6c.
HX-Shell09	IAAA-100063*	3,920 ± 30		Shell; Loc. 3; Fig. 4c.
HX-Shell10	IAAA-100064*	22,630 ± 80		Shell; Loc. 3; Fig. 4c.
HX-Shell11	IAAA-100065*	16,270 ± 50		Shell; Loc. 3; Fig. 4c.
HX-Shell12	IAAA-100068*	36,330 ± 200		Shell; Loc. 4; Fig. 6a.
HX-Shell14	IAAA-100070*	36,080 ± 190		Shell; Loc. 4; Fig. 6c.
HX-Shell15	IAAA-100071*	35,280 ± 170		Shell; Loc. 4; Fig. 6c.
HX-C04	IAAA-100072*	5,300 ± 30		Organic soil; Fig. 2b.
20110701-C03	IAAA-110681*	24,483 ± 77		Shell; Loc. 3; Fig. 4c.
20110703-C04	IAAA-110682*	2,921 ± 26	1213-1021 B.C.	Organic soil; Loc. 6; Fig. 12b.
20110703-C05	IAAA-110683*	2,590 ± 22	808-767 B.C.	Organic soil; Loc. 6; Fig. 12b.
20110703-C06	IAAA-110684*	1,145 ± 20	783-788 A.D.	Organic soil; Loc. 6; Fig. 12b
20110703-C07	IAAA-110685*	676 ± 23	1360-1388 A.D.	Organic soil; Loc. 6; Fig. 12b
20110703-C08	IAAA-110686*	30,807 ± 117		Shell; Loc. 6; Fig. 12b.
20110703-C09	IAAA-110687*	19,358 ± 60		Shell; Loc. 6; Fig. 12b.
20101029-C02	Beta-290414**	41,920 ± 440		Shell; Loc. 5; Fig. 9b.
20101029-C08	Beta-290415**	7,670 ± 50		Organic soil; Loc. 5; Fig. 9b.
20101029-C09	Beta-290416**	23,170 ± 100		Shell; Loc. 5; Fig. 9b.
20101029-C10	Beta-290417**	42,130 ± 510		Shell; Loc. 5; Fig. 9b.
20101029-C11	Beta-290418**	>43,500		Shell; Loc. 5; Fig. 9b.
20101029-C13	Beta-290419**	22,280 ± 100		Shell; Loc. 5; Fig. 9b.
20101029-C14	Beta-290420**	41,240 ± 460		Shell; Loc. 5; Fig. 9b.

[*]Samples were analyzed at the Institute of Accelerator Analysis Ltd., Japan; [**]Samples were analyzed at the BETA Analysis Inc., USA.

[†]Using Accelerator Mass Spectrometry (AMS) method, referenced to the year 1950 A.D.

[‡]Dendrochronologically calibrated calendar age by Method A from CALIB Radiocarbon Calibration Version 6.1 (Stuiver et al., 2005).

[§]Types of samples collected for ^{14}C age dating.